1 *Unraveling the Mechanism of a LOV Domain Optogenetic Sensor: A Glutamine Lever Induces*

2 *Unfolding of the Jα Helix*

3 James N. Iuliano,[†] Jinnette Tolentino Collado,[†] Agnieszka A. Gil,[⊥] Pavithran T. Ravindran, [⊥]

4 Andras Lukacs,[‡,§] SeungYoun Shin,[†] Helena A. Woroniecka,[†] Katrin Adamczyk,[‡] James M.

5 Aramini,[¥] Uthama R. Edupuganti,[¥,$] Christopher R. Hall,[‡] Gregory M. Greetham,[∥] Igor V.

6 Sazanovich,[∥] Ian P. Clark,[∥] Taraneh Daryaee,[†] Jared E. Toettcher,[⊥] Jarrod B. French,[†,±] Kevin H.

7 Gardner,[¥,&,#] Carlos L. Simmerling,[†*] Stephen R. Meech,[‡*] and Peter J. Tonge.[†*]

8 [†]*Department of Chemistry, Stony Brook University, New York, 11794, United States.* [⊥]*Department of Molecular*

9 *Biology, Princeton University* [‡]*School of Chemistry, University of East Anglia, Norwich, NR4 7TJ, U.K.* [§]*Department*

10 *of Biophysics, Medical School, University of Pecs, Szigeti út 12, 7624 Pecs, Hungary.* [∥]*Central Laser Facility,*

11 *Research Complex at Harwell, Rutherford Appleton Laboratory, Didcot, OX11 0QX, U.K.* [¥]*Structural Biology*

12 *Initiative, CUNY Advanced Science Research Center, 85 St. Nicholas Terrace, New York, NY 10031.* [$]*Ph.D. Program*

13 *in Biochemistry, CUNY Graduate Center, New York, NY;* [&]*Ph.D. Programs in Biochemistry, Biology, and Chemistry,*

14 *CUNY Graduate Center, New York, NY;* [#]*Department of Chemistry & Biochemistry, City College of New York, New*

15 *York, NY;* [±]*Hormel Institute, University of Minnesota, Austin, MN, 55912.*

16

17 *Authors to whom correspondence should be addressed:

18 Email: carlos.simmerling@stonybrook.edu (CLS); s.meech@uea.ac.uk (SRM);

19 peter.tonge@stonybrook.edu (PJT)

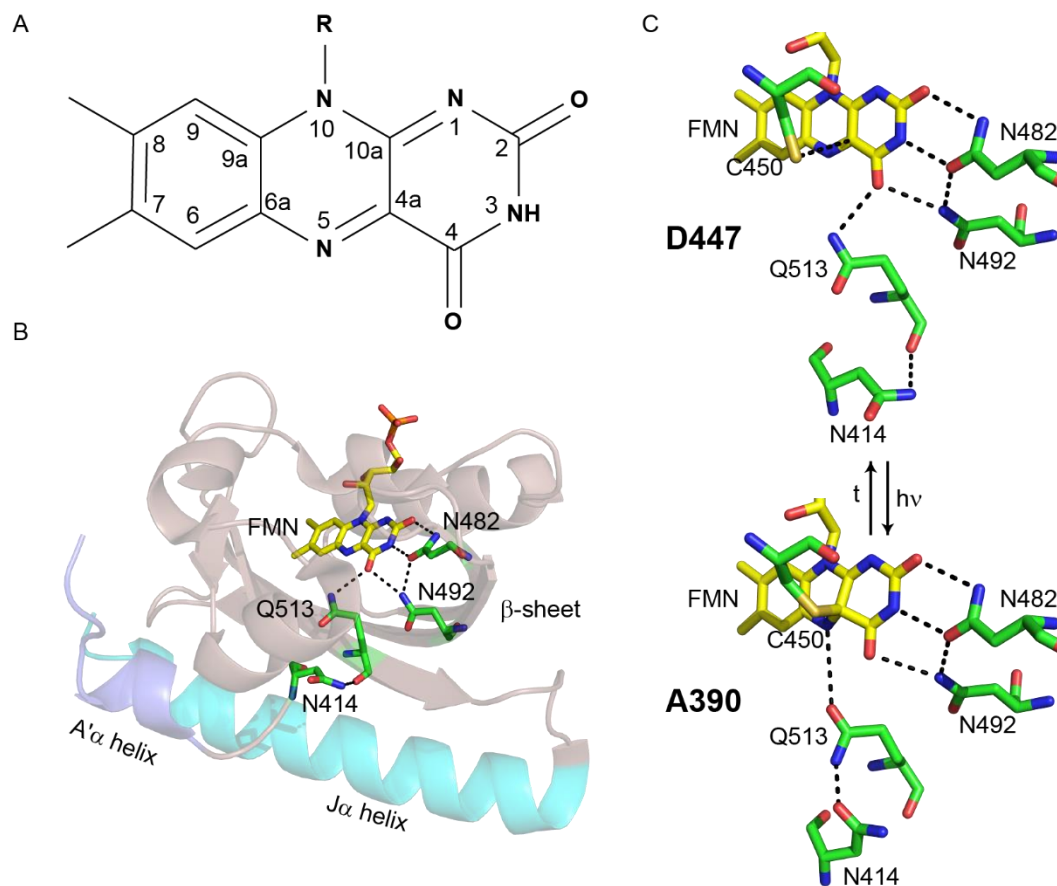20 Keywords: LOV, structural dynamics, optogenetics, flavoprotein, ultrafast IR

21

Abstract

Light-activated protein domains provide a convenient, modular, and genetically encodable sensor for optogenetics and optobiology. Although these domains have now been deployed in numerous systems, the precise mechanism of photoactivation and the accompanying structural dynamics that modulate output domain activity remain to be fully elucidated. In the C-terminal light, oxygen, voltage (LOV) domain of plant phototropins (LOV2), blue light activation leads to formation of an adduct between a conserved Cys residue and the embedded FMN chromophore, rotation of a conserved Gln (Q513), and unfolding of a helix (Jα-helix) which is coupled to the output domain. In the present work, we focus on the allosteric pathways leading to Jα helix unfolding in *Avena sativa* LOV2 (AsLOV2) using an interdisciplinary approach involving molecular dynamics simulations extending to 7 μs, time-resolved infrared spectroscopy, solution NMR spectroscopy, and in-cell optogenetic experiments. In the dark state, the side chain of N414 is hydrogen bonded to the backbone N-H of Q513. The simulations predict a lever-like motion of Q513 after Cys adduct formation resulting in loss of the interaction between the side chain of N414 and the backbone C=O of Q513, and formation of a transient hydrogen bond between the Q513 and N414 side chains. The central role of N414 in signal transduction was evaluated by site-directed mutagenesis supporting a direct link between Jα helix unfolding dynamics and the cellular function of the Zdk2-AsLOV2 optogenetic construct. Through this multifaceted approach, we show that Q513 and N414 are critical mediators of protein structural dynamics, linking the ultrafast (sub-ps) excitation of the FMN chromophore to the microsecond conformational changes that result in photoreceptor activation and biological function.

Introduction

The C-terminal light, oxygen, voltage (LOV) domain from plant phototropins are versatile protein domains that have been adapted for protein engineering and molecular imaging.[1,2] LOV photoreceptors are members of the Per-ARNT-Sim (PAS) domain superfamily and use a non-covalently bound flavin mononucleotide (FMN) cofactor to sense 450 nm (blue) light (**Figure 1A**).[3] Light excitation initiates a photocycle in which a singlet excited state undergoes intersystem crossing to a triplet excited state which subsequently forms a covalent Cys-FMN-C4a adduct on the μs timescale that absorbs at 390 nm (A390).[4] Formation of the A390 Cys adduct and accompanying protonation of the adjacent N5 position[5] are thought to be the driving force behind the structural changes that accompany effector activation in the LOV domain family including alterations in the structure and conformation of the C-terminal Jα helix.[6]

Figure 1: The AsLOV2 domain. (A) The isoalloxazine ring of the FMN cofactor. (B) The FMN cofactor (yellow) makes hydrogen bonding interactions with Q513, N492 and N482. Q513 in turn is hydrogen bonded to N414. The Jα helix is shown in cyan and the A'α helix is shown in slate. (C) The hydrogen bonding network around FMN is shown for both the dark (D447) and light (A390, adduct) states. The flipped conformation of Q513 is shown for the light state structure. The figure was made using PyMOL Molecular Graphics Software[7] using the crystal structures of AsLOV2 (PDB 2V1A (dark), 2V1B (light)).[8]

65   The LOV2 domain from *Avena sativa* phot1 (AsLOV2) is a model system for LOV

66   photoreceptor activation (**Figure 1B**). The isoalloxazine ring of the FMN cofactor is surrounded

67   by a hydrogen-bonding network that senses and responds to excitation on the ultrafast timescale

68   leading to activation of a Ser/Thr kinase that regulates phototropism in plants.[9] Photoexcitation

69   results in formation of an adduct between C450 and FMN and protonation of FMN-N5 which

70   results in rotation of a conserved Gln (Q513) and unfolding of a conserved C-terminal α helix (Jα

71   helix).[9] Structural changes are also observed in the LOV domain β-sheet,[10,11] and an N-terminal

72   helix (A'α) is thought to act as a regulatory element which unfolds concurrently with changes in

73   the Jα helix.[12,13]

74   Optogenetics and optobiology are emerging fields in which a range of biological functions can

75   now be controlled by light. Early LOV-effector fusions were constructed to afford light control to

76   the enzyme dihydrofolate reductase[14], transcription repressors[15], and histidine kinases.[16] Fusion

77   proteins utilizing AsLOV2 followed, with the development of the photo-activatable LOV-Rac1

78   sensor (PA-Rac1) in which the Jα helix was used as a reversible photocage controlling the activity

79   of the GTPase Rac1.[17,18] Further protein engineering led to the development of iLID, which added

80   light inducible dimerization capabilities and a recognition peptide embedded within the sequence

81   of the Jα helix such that unfolding of the Jα helix enabled recruitment of signaling proteins in-

82   cell,[19] and LEXY, which included a nuclear export sequence in the Jα helix so that nuclear export

83   could be controlled by blue light.[20] Despite these advances, some LOV-based optogenetic tools

84   still possess a significant level of activity in the dark state, resulting in sub-optimal dynamic range

85   and limiting their broad deployment. A complete molecular understanding of the mechanism of

86   LOV domain function is thus required for the rational optimization of LOV-based optogenetic

87   photoreceptors.[21,22]

Molecular dynamics (MD) simulations have previously guided hypotheses into the mechanism of formation,[23] and breakdown,[24] of the Cys-FMN adduct, and the accompanying structural dynamics,[13,25] in native LOV domains and mutants lacking the Cys residue.[26] Initial studies by Peter et al. focused on the role of the Iβ and Hβ strands in signal propagation,[25] resulting in the proposal that stress on Iβ leads to rearrangement of the hydrogen bonding contacts between Hβ and the Jα helix and helix unfolding. It was also proposed that the FMN binding pocket undergoes dramatic changes in which N482 and N492 move out of the pocket to maintain contacts between Q513 and FMN. Freddolino et al. extended this work by increasing the simulation timescale to 1 μs,[13] leading to the identification of a potential salt bridge between the A'α and Jα helices, and supporting previous studies of an interaction between the two helices. The simulations also suggested that the N414 side chain N-H forms a H-bond with the Q513 side chain C=O during light state formation. The role of N414 in photoactivation has been tested experimentally in which the N414A, N414V and N414Q mutations modulate the cycling time of AsLOV2 with time constants of 1427 s, >720 s, and 280 s, respectively compared to 80 s for wild-type.[27] In the case of N414V, a slightly unfolded Jα helix was observed in the dark state.[12]

LOV structural dynamics have been studied extensively using infrared spectroscopy and more recently time-resolved infrared spectroscopy (TRIR). A marker band for unfolding of the Jα helix was identified in the amide I region, ~1620-1640 cm^{-1} using difference FTIR.[28–30] TRIR experiments revealed that helix unfolding was multi-step,[31] and that structural changes resulting from adduct formation follow dispersive kinetics commonly associated with sampling of multiple protein conformations prior to reaching a metastable state, which is the signaling state in LOV domain proteins.[32] TRIR spectroscopy of multiple LOV domain proteins revealed variations in the dynamics of the β-sheet and the Jα helix, which link the LOV domain to the relevant effector

111   domains.[33] Despite the information obtained from time-resolved spectroscopy, the mechanisms

112   of signal propagation from FMN to the effector domain are still largely unknown.

113   Using a combination of theoretical and experimental approaches, we have now directly probed

114   the evolution of the structural dynamics in AsLOV2 that couple flavin photoexcitation with

115   structural changes at sites that are remote from the chromophore.   In particular, we have

116   determined that the rotation of Q513 out of the flavin binding pocket and the formation of a

117   transient hydrogen bond with N414 is a key step in the mechanism of Jα helix unfolding. Site

118   directed mutagenesis combined with time-resolved infrared spectroscopy and NMR spectroscopy

119   was used to interrogate this mechanism and we found that the Jα helix was partially unfolded in

120   the dark state and unfolding kinetics were accelerated in the N414A mutant and delayed in N414Q

121   AsLOV2. To correlate photoreceptor dynamics and function, the impact of the mutants was

122   assessed at the cellular level in the Zdk2-AsLOV2 dimerization (LOVTRAP) system where it was

123   found that the N414A mutant showed a 4-fold reduction in activity and dynamic range when

124   exposed to blue light.

125

Results

126

The objective of this work was to characterize the structural dynamics that lead to Jα helix

127

unfolding in AsLOV2. To accomplish this goal we used MD simulations to analyze the structural

128

changes that accompany light state formation by inserting the Cys-FMN light state adduct into the

129

dark state structure of AsLOV2 and then allowing the MD simulations to 'relax' the protein

130

structure to adjust to the presence of the Cys-FMN adduct. The MD simulations were used to

131

identify key residues implicated in the pathway leading to Jα helix unfolding. Site-directed

132

mutagenesis was then used to probe the role of these residues in light state formation and AsLOV2

133

dynamics using a combination of MD simulations, static and time-resolved infrared spectroscopy,

134

$^{15}N/^1H$-HSQC NMR spectroscopy, and cell-based optogenetic experiments. Based on this analysis

135

we propose a mechanism for photoactivation in which a hydrogen bonding interaction between the

136

NH side chain of N414 and backbone C=O of Q513 is broken and a transient hydrogen bond is

137

formed between the NH and C=O side chain groups of N414 and Q513, respectively. Q513 is thus

138

shown to act as a lever which forces the Jα helix away from the LOV domain thereby initiating

139

helix unfolding and activation of the downstream effector module.

140

141

Molecular dynamics (MD) simulations of AsLOV2

142

To identify allosteric pathways leading to unfolding of the Jα helix in AsLOV2, we used

143

MD simulations to predict structural changes in response to Cys-FMN formation. The Cys-FMN

144

adduct was taken from the light state crystal structure (PDB 2V1B),[8] and parameterized prior to

145

insertion into the dark state crystal structure (PDB 2V1A). The dark state crystal structure

146

containing the light state Cys-FMN adduct was equilibrated prior to the MD simulations which

147

148   were then performed in 4 fs steps for >7 μs to simulate the response of the protein to Cys-FMN

149   adduct formation.

150   The data from the simulations are presented as a heat map in **Figure 2A** with time on the

151   x-axis, residue number on the y-axis, and a color bar to show increasing root mean squared

152   deviation (RMSD, log scale) from the initial dark state structure. The simulation reveals that

153   residues in a loop immediately preceding the Jα helix become perturbed by adduct formation early

154   in the simulation and propagate through the N-terminal end of the Jα helix with the most dramatic

155   changes in the helix occurring at ~5 μs with complete loss of helical character. The simulation was

156   run with the same forcefield on the dark state (cysteine adduct not formed) where it was predicted

157   that the Jα helix is stable for the 9.25 μs of simulation time (**Figure S3**).

158
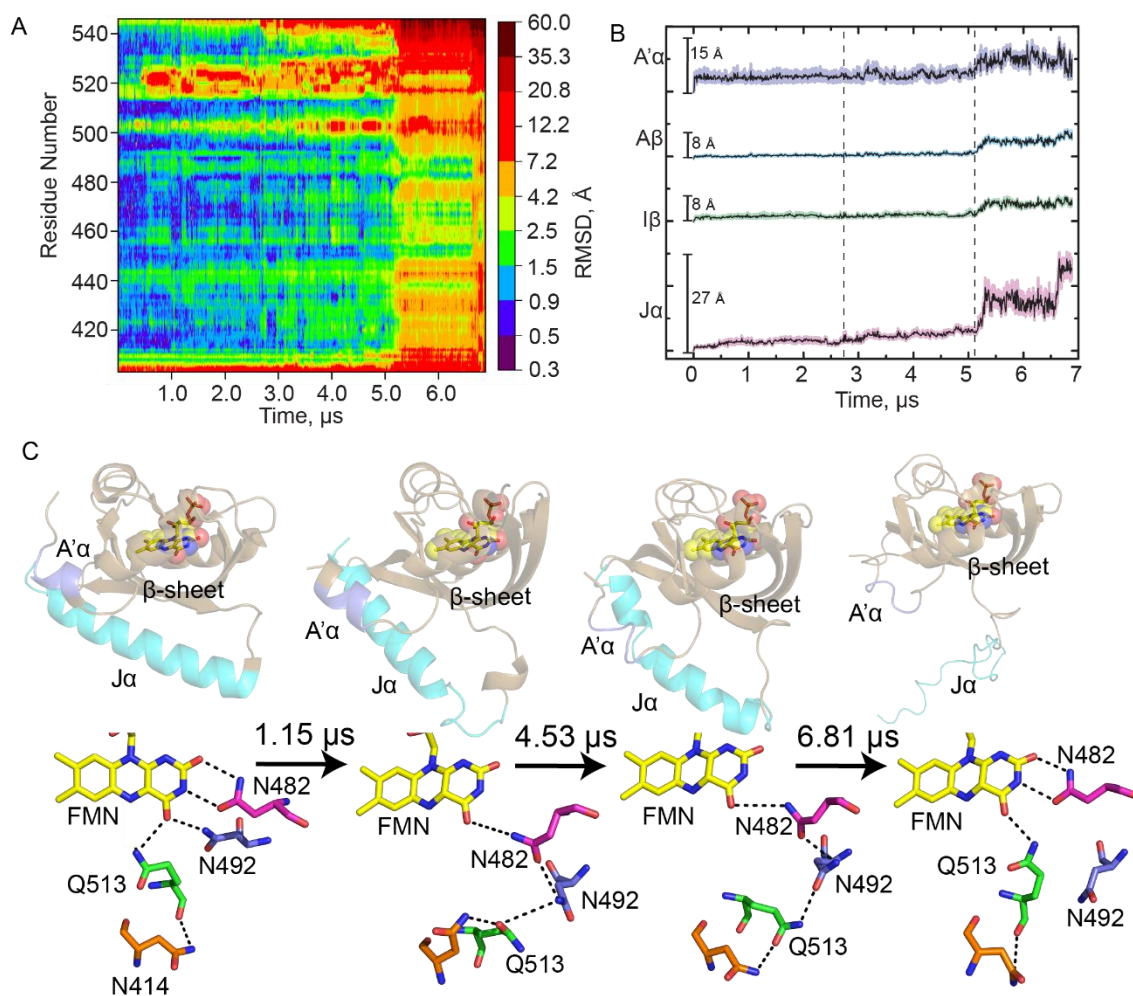
Figure 2: Molecular dynamics simulations reveal hydrogen bonding pathways leading to Jα helix unfolding. (A) RMSD as a function of time post-adduct formation for each residue in AsLOV2 is shown as a heat map with increasing simulation time on the x-axis and residue number on the y-axis. A color bar shows increasing RMSD in Å from the initial dark state structure. (B) Average RMSD ± SEM for select structural components of the LOV domain: A'α helix (slate), Aβ (cyan), Iβ (green), and Jα (pink). (C) The evolution in secondary structure is shown together with changes in hydrogen bonding interactions between the flavin and residues N482, N492, Q513 and N414 for post-adduct formation simulation times of 0 (dark state AsLOV2, 2V1A), 1.15 μs,

10

169   4.53 µs, and 6.81 µs (Light state, MD). Hydrogen bonds are shown as black dotted lines. The

170   figure was made using PyMOL Molecular Graphics Software[7] using predicted structures from MD

171   simulations performed in Amber.[8,40]

172

173

174   Averaged RMSD traces as a function of time are shown for several key regions of AsLOV2

175   with maximum RMSD shown as a scale bar (black line, **Figure 2B**). The standard error of the

176   mean (SEM) is shown as shaded color around the black line. The A'α helix (residues 404-410,

177   slate) shows the most variability very early in the simulation with both high average RMSD and

178   SEM, consistent with previous experimental work.[12] The RMSD increases again at 5 µs, on the

179   timescale of unfolding of the Jα helix. RMSD for the β-sheet (Aβ (residues 414-418, cyan) and Iβ

180   (residues 506-516, green)) are also shown and predict significant perturbations after 5 µs. The Jα-

181   helix (residues 522-544, pink) shows the most changes in RMSD over time, as expected for the

182   helical to disordered transition that has been shown to occur upon light state formation by Gardner

183   and others.[9,50] The unfolding of the Jα helix appears to occur in four phases with increases in

184   RMSD at 0.5 µs, 2.75 µs, 5.25 µs, and 6.60 µs. The 0.5 µs phase involves the initial undocking of

185   the Jα-helix from the β-sheet (**Figure 2C, S1**) and the formation of a helical structure in the loop

186   adjacent to the Jα helix (1.15 µs snapshot). These events appear to be initiated by the rotation of

187   Q513. The 5.25 µs phase is assigned to more significant disordering of the Jα helix which results

188   in complete unfolding of the helix by ~6.60 µs.

189   The changes in secondary structure are accompanied by specific changes in the residues

190   that surround the FMN chromophore and are presented as snapshots from the MD trajectories

191   **(Figure 2C)**. These snapshots were chosen to represent sections of the trajectory where increase

192   in the RMSD are observed (vertical dashed lines). In the dark state N414 is hydrogen bonded to

193   the backbone amide of Q513. By the 0.38 µs time point of the simulation Q513 is predicted to

194   move 2.4 Å and 5.7 Å from its initial backbone and side chain positions, respectively, and rotate

195   62° out of the binding pocket. This motion of Q513 pulls the β-sheet such that the side-chains of

196   N482 and N492 lose their hydrogen bonding interactions with C2=O, C4=O, and N3-H of FMN.

197   In the 4.53 µs structure, N482 appears to undergo a 3.1 Å slide out of the pocket while N492

198   rotates outward by 31° resulting in a side chain motion of 3.7 Å. These residues appear to form a

199   chain that includes N414, Q513, N492, and N482 in which N482 remains hydrogen bonded to the

200   flavin C4=O (Figure 2C, 1.15 µs and 4.53 µs structures), consistent with simulations by Freddolino

201   et al.[13] N482 appears to move back toward C2=O over time while N492 undergoes a rotation

202   along the protein backbone and remains rotated out and exposed to solvent (between 1.15 µs to

203   6.81 µs). In the 6.81 µs structure, N482 has returned to its initial dark state position while N492

204   is predicted to remain rotated out of the pocket, 4.4 Å from its initial position. Q513 is shown to

205   be hydrogen bonded to C4=O, though in a slightly different orientation compared to that observed

206   in the X-ray structure of the light state (**Fig S2**). The differences can be explained by the method

207   of generating light state crystals in which the protein crystals of the dark state were illuminated

208   prior to data collection and may not reflect the flexibility of the protein observed in solution

209   measurements. Simultaneously, N414 is pulled away from Q513 due to its proximity to the A'α

210   helix which becomes disordered prior to unfolding of the Jα helix. We propose that the transient

211   hydrogen bond between N414 and Q513 links A'α to FMN C4=O via a 15 Å signal transduction

212   wire in which N482 and N492 maintain a connection between Q513 and FMN. This in turn results

213   in unfolding of the A'α helix concomitant with distortion of the β-sheet such that the Jα helix is

214   pushed far enough away from the LOV core to induce its unfolding.

215

A transient hydrogen bond between Q513 and N414 modulates helix unfolding.

The MD results were used to inform fs-ms TRIR measurements, suggesting transient studies of N414A and N414Q-AsLOV2 mutants could provide valuable insight into Jα helix unfolding dynamics. The N414A mutation was chosen to remove potential hydrogen bond interactions with the N414 side chain and the N414Q mutation was chosen to retain an amide side chain potentially capable of forming a hydrogen bond with Q513.

We first measured the TRIR spectra of wild-type AsLOV2 using time resolved multiple probe spectroscopy (TRMPS, **Figure 3A**). The band assignments and time constants of 2.3 ns, 8.8 μs, and 14 μs corresponding to the excited state decay, triplet state decay, and A390 formation are consistent with the global analysis of our previous data from Gil et. al. (**Figure 3B**).[32] A fourth, 313 μs time constant (EAS5) has been added to the global fitting model for wild-type AsLOV2 which describes the formation of the final signaling state as observed in light minus dark (L-D) steady state FTIR measurements (**Figure 3B; Figure S5** shows the comparison between EAS5 and L-D FTIR). This additional EAS5 is termed "Sig" and corresponds to full disordering of the helix and light state formation. The bleach at 1626 cm^{-1}, which corresponds to disorder of the Jα helix, reaches a maximum of -0.35 mOD on this timescale and does not recover within the time resolution of the experiment (**Figure 4A**). The transient at 1636 cm^{-1} shows a rise and decay on the μs timescale assigned to an intermediate state between adduct formation and Jα helix unfolding, and consistent with the presence of a transient hydrogen bond from the MD simulations. Therefore, the full activation pathway of AsLOV2 can be probed using the TRMPS method.
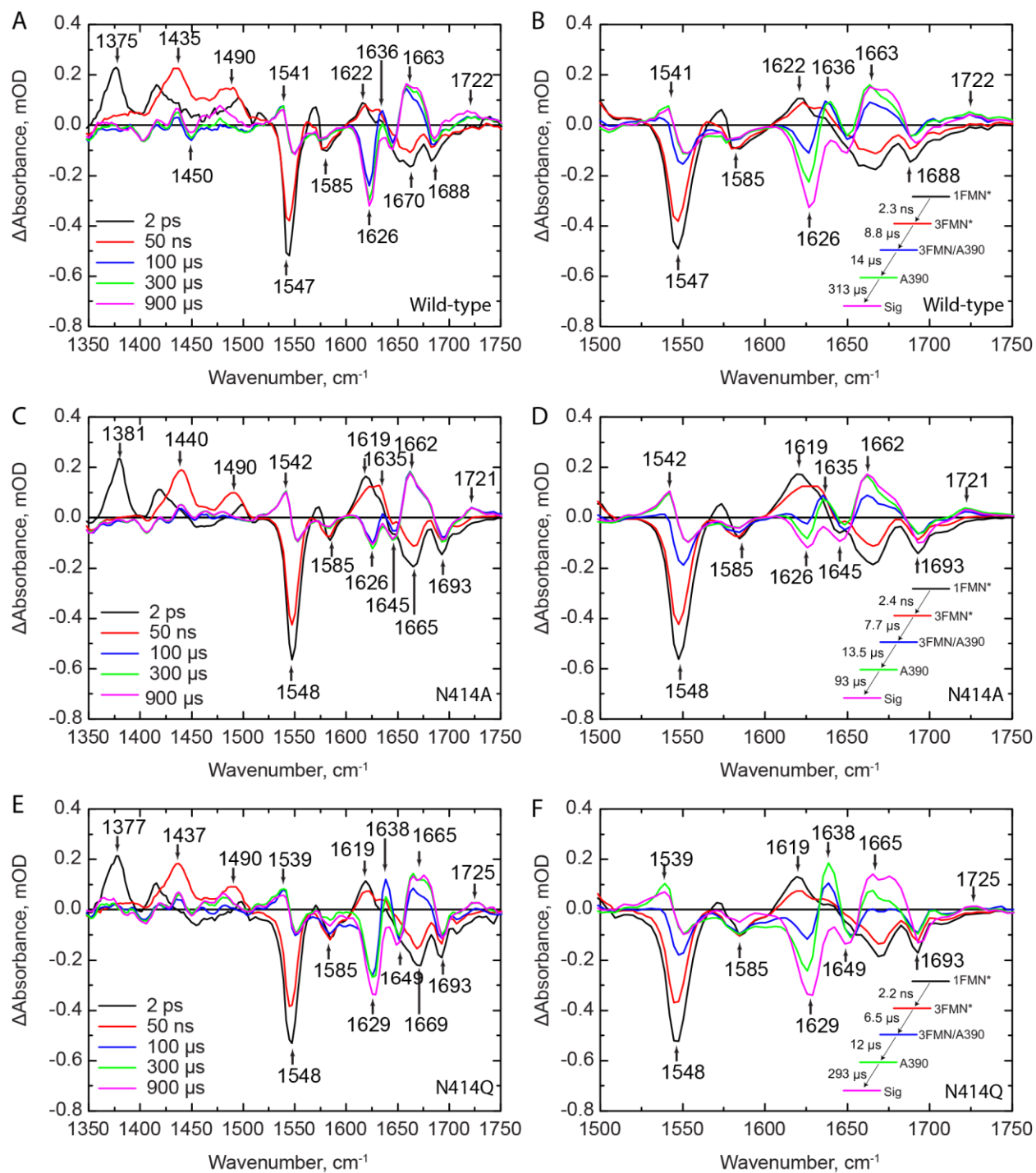
Figure 3: TRIR spectra of wild-type and mutant AsLOV2 proteins shows reduced helix unfolding in N414A-AsLOV2. TRIR spectra for (A) wild-type, (C) N414A, and (E) N414Q-AsLOV2 are shown at time delays of 2 ps, 50 ns, 100 μs, 300 μs, and 900 μs. The EAS from a

240   global fit to a sequential exponential model are shown adjacent to the respective TRIR panels B,

241   D, and F, respectively. While the excited and triplet state decays are not affected by mutation of

242   N414, there is a 3-fold acceleration in the rate of formation of the final Sig state in N414A

243   AsLOV2. The N414 -AsLOV2 mutant also shows reduced changes in the 1626 cm^{-1} band assigned

244   to the Jα helix while N414Q AsLOV2 shows a reduced rate of structural dynamics and larger

245   amplitude of the 1638 cm^{-1} band in the A390 state.

246

247

248   We then measured the TRIR spectra of N414A and N414Q AsLOV2 (**Figure 3C,E**).

249   Whilst the excited state (^{1}FMN* and ^{3}FMN*) spectra and kinetics are identical to those of the

250   wild-type protein, the changes to N414 result in dramatic differences in the A390 to Sig EAS. In

251   N414A AsLOV2 (**Figure 3C,D**), the bleach at 1626 cm^{-1} corresponding to the disordered Jα helix

252   is reduced ~3-fold in intensity to -0.12 mOD, suggesting that the changes in Jα are reduced and

253   partially decoupled from chromophore activation (**Figure 4A, red trace**). The transient at 1635

254   cm^{-1} is still evolving in a similar manner to that observed in the wild-type protein, although the

255   rise in the transient is not as pronounced in the N414A mutant **(Figure 4B)**. In addition, the time

256   constant for evolution of the A390 to Sig states is accelerated ~3-fold to 93 μs compared to the

257   313 μs time constant determined for wild-type AsLOV2. This suggests that the final "Sig" state

258   forms faster in N414A AsLOV2, further suggesting altered structural dynamics in this mutant.

259   In the N414Q mutant, the amide side chain of N414 is conserved by mutation to Q414,

260   preserving the potential for formation of a transient hydrogen bond. The EAS are shown in Figure

261   3F. While overall very similar to the wild-type AsLOV2, there are several results that deserve

262   comment. The time constant determined for the A390 to Sig EAS is 293 μs, which is very similar

263   to that of the wild-type at 313 µs. However, the transient at 1636 cm^{-1} in N414Q is larger than that

264   of the wild-type as shown in the raw µs-timescale data (**Figure 3F**), suggesting that the helix is

265   more stable in the dark state but ultimately unfolds at a similar rate to the wild-type protein. Based

266   on these data, we hypothesize that the 1636 cm^{-1} transient can be assigned to the Q513 side-chain

267   carbonyl itself, or at least that dynamics associated with this signal directly report on the hydrogen

268   bond between N414/Q414 and Q513.

269
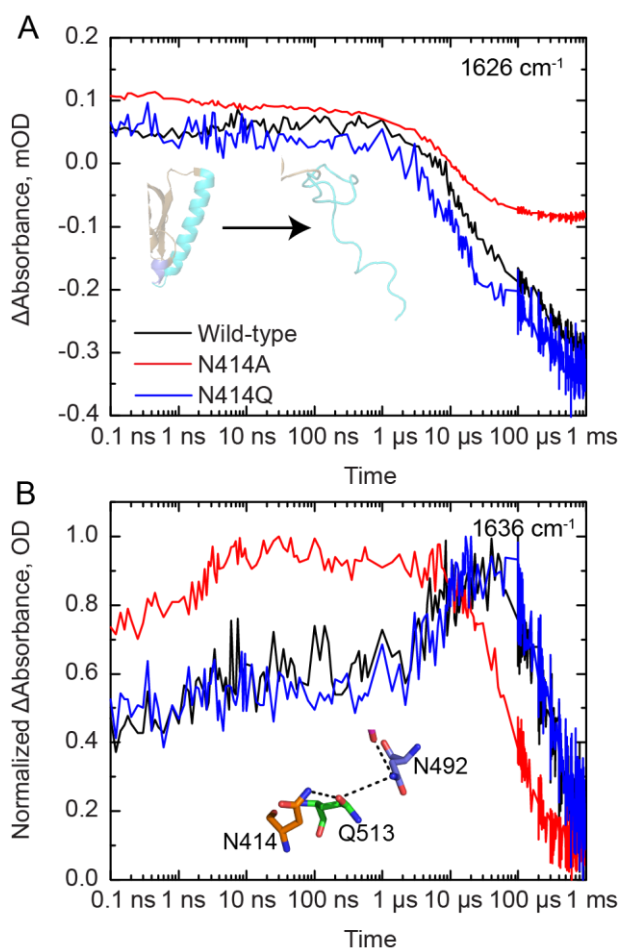
270

271   **Figure 4: Selected kinetic traces from TRIR spectra of wild-type and mutant AsLOV2.** (A)

272   The unfolding of the Jα helix is tracked by the increase in bleach intensity at 1626 cm^{-1} for the

273   wild-type (black), N414A (red) and N414Q (blue) AsLOV2 proteins. (B) A rise and decay of the

274   signal at 1636 cm^{-1} is assigned to structural dynamics associated with a transient hydrogen bond

275   between N414 and Q513 due to the rotation of Q513. This signal decays to zero with the time

276   constant of the fourth EAS.

277

278

279   *^{15}N/^{1}H-HSQC NMR Reveals the Jα helix is primed for unfolding in N414A AsLOV2*

280   As the TRIR and FTIR are difference experiments that show changes in the protein due to light

281   activation, we used ^{15}N-HSQC NMR to characterize the Jα helix in wild-type, N414A, and N414Q

282   AsLOV2 in both dark and light states (**Figure S8, S9, and S10**, respectively). Excitation of wild-

283   type AsLOV2 with 488 nm light reveals the formation of cross peaks between resonances at 7.5

284   and 8.5 ppm, consistent with the data reported by Harper et al.[9] In N414A AsLOV2, some of these

285   cross peaks are already formed in the dark state (**Figure S9**), suggesting that N414A AsLOV2 is

286   in a structurally primed state for photoactivation with some residues in active or partially active

287   conformations. The 2D NMR spectrum of N414Q AsLOV2 resembles wild-type-AsLOV2 in that

288   there is clear separation between peaks from 7.5 and 8.5 ppm that become more poorly resolved

289   upon light activation (**Figure S10**).

290

291
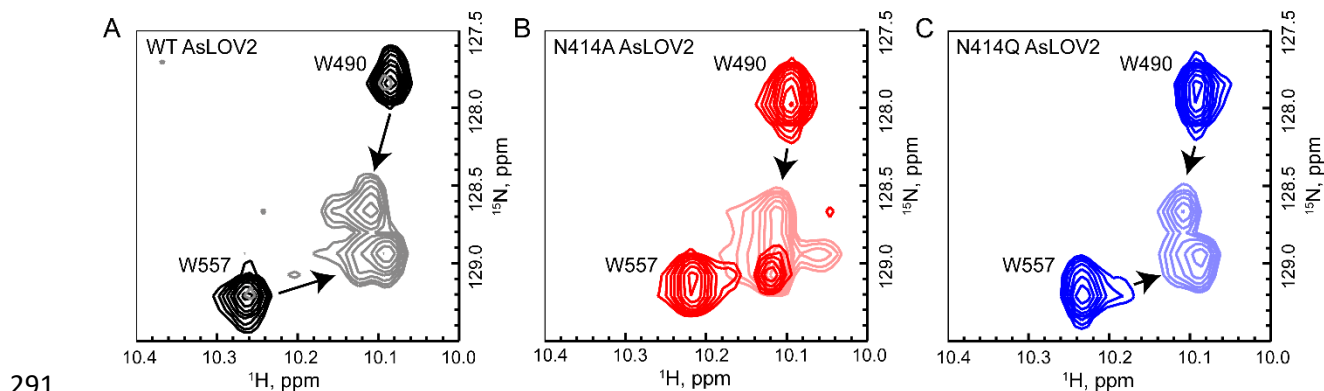
Figure 5: ^{15}N/^{1}H-HSQC NMR reveals that the Jα helix is partially unfolded in N414A-AsLOV2. (A) Tryptophan indole side-chain chemical shifts of the wild-type protein show a clear shift and broadening from dark to light states (black to gray). (B) The same resonances in N414A AsLOV2 show that W557, which is located on the Jα helix, is partially in the lit state suggesting that the helix is partially unfolded (Dark red to light red). (C) N414Q AsLOV2 does not show partial unfolding, however the peak assigned to W557 is distorted compared to wild-type AsLOV2 (Dark blue to light blue).

The indole side chains of W491 and W557 have been previously shown to be sensitive to the structure of the Jα helix.[9] The W491 side chain is located near the N-terminal end of the Jα helix while W557 is located on the Jα helix itself. Wild-type AsLOV2 shows a clear change in the chemical shifts of both Trp residues between the dark and light states (**Figure 5A**). The W491 indole side chain N-H has chemical shifts of 10.09 ppm (^{1}H) and 127.75 ppm (^{15}N) in the dark state and 10.12 ppm (^{1}H) and 128.6 ppm (^{15}N) in the light state, whereas W557 has chemical shifts of 10.26 ppm (^{1}H) and 129.25 ppm (^{15}N) in the dark state and 10.10 ppm (^{1}H) and 129.00 ppm (^{15}N) in the light state. In the dark state of N414A AsLOV2 there is a population of W557 that has chemical shifts similar to those observed in the light state while W491 has a similar chemical shift, albeit shifted to 128.00 ppm (^{15}N), compared to wild-type AsLOV2 (**Figure 5B**). This suggests that the C-terminal end of the Jα helix is slightly unfolded due to mutation of N414 while the hinge-loop region connecting the Jα to the LOV core is intact. The disorder of the Jα helix in the N414A AsLOV2 dark state observed in these HSQC spectra is consistent with the smaller 1626 cm^{-1} bleach in the TRIR experiment suggesting that the helix is partially unfolded in the dark state.

315

A cell-based assay shows loss of function associated with changes in Jα helix unfolding of the

N414 mutants

  To assess the functional consequences of mutating N414, we used the cell-based

LOVTRAP system to measure the ability of AsLOV2 to dimerize to the plasma membrane

localized Zdk2 protein and release from the plasma membrane upon light activation (**Figure 6A**).[51]
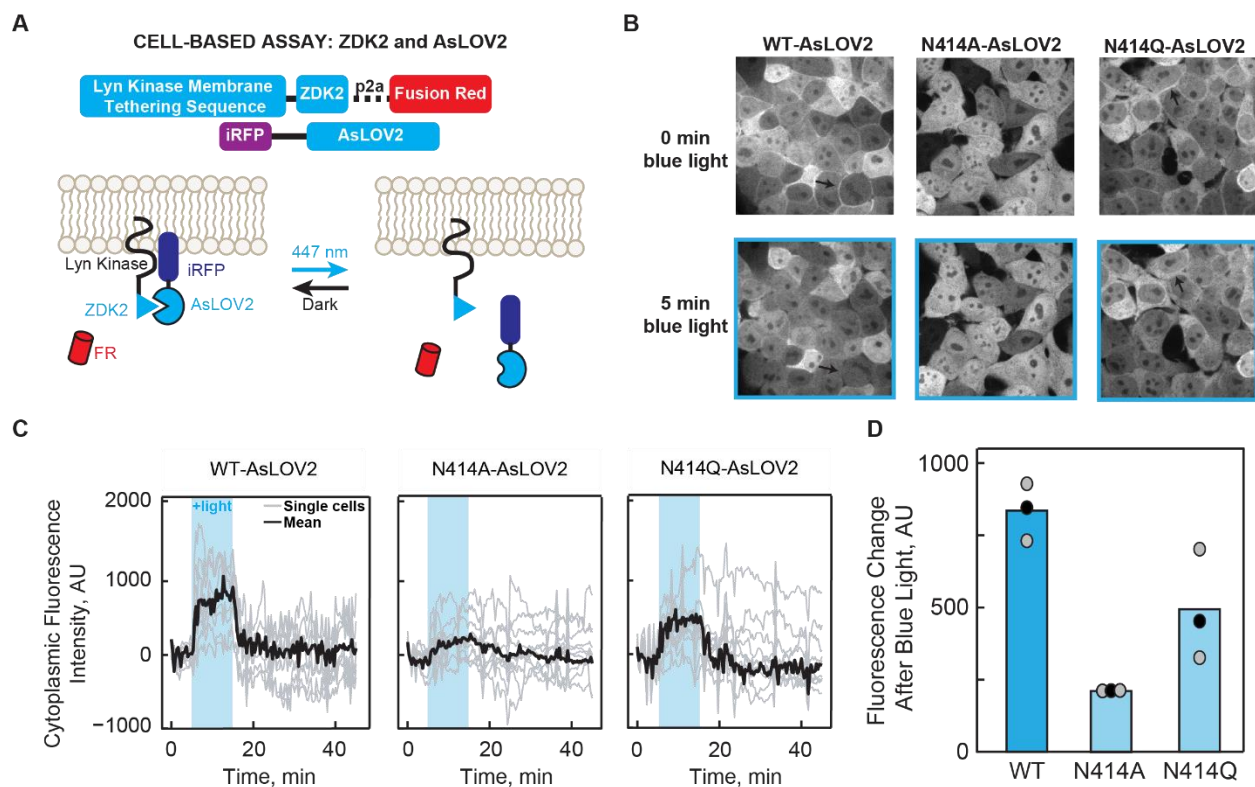
Figure 6: LOVTRAP assay shows altered Jα helix dynamics in N414A AsLOV2. (A)
Schematic diagram of the LOVTRAP system. The Zdk2 domain binds to the Jα helix of AsLOV2
in the dark state and is released upon illumination with 447 nm light. The translocation of AsLOV2
is tracked using iRFP. (B) Representative images showing the localization of AsLOV2 to the
plasma membrane in the dark state and diffusion into the cytoplasm after 5 min of blue light

19

328   illumination. Localization on the plasma membrane is shown by black arrows. Fluorescence

329   localization to the cell membrane can be observed in wild-type AsLOV2 and N414Q AsLOV2 but

330   not N414A AsLOV2 in the dark state. Fluorescence localization to the cell membrane is not

331   observed for the AsLOV2 variants after blue-light irradiation. (C) Quantification of the change in

332   fluorescence in the cytoplasm over time shows that N414A AsLOV2 has reduced light-induced

333   localization and ΔF compared to wild-type and N414Q AsLOV2. (D) Quantification of the total

334   maximum change in fluorescence due to release of AsLOV2 from the membrane. Each point

335   represents the average of 10 cells after 8 minutes of blue light exposure. The mean and standard

336   deviations of each bar are shown as black and gray dots, respectively.

337

338

339   Localization of AsLOV2 to the plasma membrane is visualized by fusion of iRFP to the

340   N-terminus of AsLOV2. For wild-type and N414Q AsLOV2, localization of the fluorescence

341   signal is observed on the plasma membrane in the dark state and is released into the cytoplasm

342   upon blue-light illumination (**Figure 6B**, black arrows denote plasma membrane) whereas the

343   N414A variant shows minimal localization to the plasma membrane even in the dark state. This

344   suggests that prior to illumination, N414A AsLOV2 exhibits light state activity. Quantification of

345   the change in fluorescence intensity in the cytoplasm over time is shown in Figure 6C for all three

346   AsLOV2 variants. The largest change in fluorescence intensity (ΔF) after illumination is observed

347   in wild-type AsLOV2 with a mean ΔF of 835±57 units, while N414Q AsLOV2 shows a slight

348   (1.7-fold) reduction in ΔF (493±110 units). These results are consistent with the NMR spectra in

349   which the chemical shift of W557 in N414Q AsLOV2 shows more disorder compared to wild-

350   type AsLOV2. N414A AsLOV2 shows a more dramatic 4-fold reduction in ΔF of 209±5 (**Figure**

351   **6D**) consistent with minimal membrane localization in the dark state. The reduced ΔF is indicative

352   of reduced dynamic range in N414A AsLOV2, either a result of the partially unfolded helix in the

353   dark state causing residual light state activity or a deficient unfolding of the Jα helix.

354   The decay of the fluorescence signal was fit to a single exponential function to determine

355   the rate of dark state recovery of the LOVTRAP construct and was found to be 60 s $\pm$ 10 s and 205

356   s $\pm$ 28 s for the wild-type and N414Q AsLOV2 proteins, respectively (**Figure S11**). These time

357   constants correlate with the solution measurements of Zayner et al.[27] in which rates of 80 s and

358   280 s were observed for wild-type and N414Q. N414A was not included in our analysis due to

359   the small change in fluorescence between dark and light states (ΔF). The faster rate of recovery

360   in the optogenetic experiment is likely due to the increased temperature from 22°C in the solution

361   experiment to 37°C in the cell-based assay.

362

363   **Discussion**

364   Photoactive proteins convert light energy into structural changes that drive and control

365   biological processes by modulating the activity of downstream output partners.[52] In the LOV

366   domain proteins the light absorbing chromophore is the isoalloxazine ring of a non-covalently

367   bound FMN cofactor. Excitation of the chromophore triggers a photocycle in which an early event

368   is the formation of a covalent adduct between the FMN and a conserved Cys residue (C450) and

369   protonation of FMN-N5.[3] Cys-FMN adduct formation then results in slower time-scale structural

370   changes that are transmitted through a C-terminal helix, the Jα-helix.[9] In AsLOV2 the helix

371   unfolds on the micro-millisecond timescale, and there have been numerous efforts to determine

372   how the Cys-FMN adduct formation modulates the structure of the helix which is ~13 Å away.[8]

373   In the current work we use a combination of MD, TRIR spectroscopy, NMR spectroscopy, site-

374 directed mutagenesis and cell-based experiments to elucidate the pathway through which the

375 chromophore and helix communicate.

376 X-ray structural studies have revealed that a conserved Gln, Q513, rotates during

377 photoactivation. In the dark state, the side-chain NH_2 and main chain C=O of Q513 are hydrogen

378 bonded to the FMN C4=O and side chain of N414, respectively, whilst in the light state, the side

379 chain carbonyl of Q513 now accepts a hydrogen bond from the protonated FMN-N5 (**Figure 1**).

380 Rotation of Q513 is clearly a key event in light state formation since replacement of this residue

381 with any other amino acid, even Asn, results in loss of photoactivity, and a series of studies have

382 shown that this motion of Q513 is coupled to later events of the photocycle, beyond 20 µs.[32] For

383 example, whilst the bleach corresponding to Jα helix unfolding is not observed by steady state

384 FTIR difference spectroscopy in the Q513L variant,[11] studies by our group using TRIR

385 spectroscopy have shown that the early steps of the photocycle (<10 µs) are not affected by

386 mutation of Q513 to Ala. Previous MD simulations have provided additional insight into the role

387 of Q513, suggesting the formation of a hydrogen bond between the Q513 side chain C=O and the

388 N414 side chain N-H group. However, these simulations were limited to 1 µs and were not able

389 to capture the unfolding of the Jα helix.[13] Recent MD simulations focused on the equivalent Gln

390 residue in Vivid predicted rotation of 180° and was shown to be required for light-induced

391 dimerization.[53]

392 In the present work we have extended the MD simulations to 7 µs which is sufficient to capture

393 unfolding of the Jα helix and provide an atomic-level prediction of the events leading to light state

394 formation. The simulation predicts a 62° rotation of the Q513 side chain leading to the formation

395 of a transient hydrogen bond between the Q513 and N414 side chains 1.15 µs after adduct

396 formation, which is accompanied by a 3.1 Å movement of N482 out of the FMN binding pocket

397 and a 31° rotation of N492 , consistent with previous MD simulations.[13] Unfolding of the Jα helix

398 occurs over the lifetime of the transient Q513-N414 hydrogen bond, and the subsequent

399 reorganization of key residues in and around the FMN binding site provide novel insights into the

400 allostery of LOV domain activation in which N482 returns to its initial conformation whilst N492

401 remains rotated out of the flavin binding pocket and does not recover on the timescale of the

402 simulation. While the H-bond network partially recovers by the end of the simulation, the Jα helix

403 remains unfolded. Thus the 7 µs simulation provides insight into the complete photoactivation

404 pathway by visualizing how the motion of the amino acids trigger larger secondary structural

405 dynamics.

406   Recent structural studies of OdAureo1a bound to 5-deaza-FMN have also shown evidence

407 of hydrogen bonding between Q513 and N414 (**Figure S12**), however the protein was found to be

408 unable to dimerize as C5 in 5-deaza-FMN cannot be protonated and was therefore photoinactive.[54]

409 Using TRIR and NMR, we have shown experimentally that the N414 amide side chain is a key

410 regulator of Jα helix unfolding through site-directed mutagenesis. In the N414A mutant, the TRIR

411 showed a diminished bleach at 1626 cm^{-1} assigned to Jα helix unfolding (**Figure 3B,E**) and the

412 time constant for the structural evolution from A390 to the final signaling state was accelerated

413 ~3-fold (Figure 4A). In contrast the N414Q mutant, which retains the amide side chain, is similar

414 to wild-type AsLOV2. Since the TRIR experiment is a difference experiment and does not

415 explicitly reveal the absolute dark and light state structures, we used NMR spectroscopy to

416 determine the structure of the Jα helix in the dark and light states of N414A and N414Q AsLOV2

417 using the indole side chain N-H groups of W491 and W557 as probes.[10] The HSQC NMR data

418 showed that the W557 side chain in the N414A AsLOV2 dark state was populating the light state

419   conformation and thus that the Jα helix is already partially unfolded in the dark state explaining

420   the smaller change in the TRIR difference spectrum for this mutant (**Figure 5**).

421   In order to link the structural dynamics revealed by the MD simulations and spectroscopic

422   studies with LOV domain function, we assessed the impact of the N414 mutations on the activity

423   of an optogenetic LOV domain construct in the cell-based LOVTRAP assay. In the dark state,

424   AsLOV2 is localized to the cell membrane due to interactions between the Zdk2 peptide/Lyn

425   Kinase Transmembrane domain fusion and the Jα helix of AsLOV2 while in the light state,

426   unfolding of the Jα helix causes dissociation of the complex and diffusion of AsLOV2 into the

427   cytoplasm, which is visualized by iRFP fluorescence. While the wild-type and N414Q construct

428   show localization to the cell membrane in the dark state and dissociation from the membrane upon

429   illumination with blue light, the N414A mutant is minimally localized to the membrane in the dark

430   state consistent with a reduction in the change in iRFP fluorescence upon illumination (**Figure 6**).

431   These results directly implicate N414 as a key regulator of LOV domain function by coupling

432   initial structural changes around the chromophore to Jα helix unfolding and photoactivation.

433   Taken together, our studies reveal that N414 plays two roles in the photoactivation

434   dynamics of AsLOV2, by directly controlling the structure of the Jα helix in the dark state, and by

435   coupling local structural changes around the FMN chromophore on light absorption with Jα helix

436   unfolding. In the dark state, the side chain of N414 is hydrogen bonded to the backbone amide of

437   Q513.[8] This appears to stabilize the interaction between A'α and Jα, which was previously shown

438   by Zayner and coworkers to be important for the unfolding of the Jα helix as observed by FTIR.[30]

439   The TRIR and NMR spectra show that N414 is responsible for stabilizing the Jα helix in the dark

440   state and that this helix is partially unfolded in the N414A mutant which has a critical impact on

441 LOV domain function since the N414A LOVTRAP mutant has lost the ability to interact with the

442 Zdk2 peptide in a light dependent manner.

443   N414 also modulates the kinetics protein evolution that occurs between Cys-FMN adduct

444 formation (A390) and Jα helix unfolding (Sig). The rise and decay pattern observed in the 1635

445 cm^{-1} band in the TRIR is consistent with the formation and breakage of structures involving amide

446 carbonyl groups. Since these kinetics are not observed in N414A, we assign the 1635 cm^{-1} band to

447 protein dynamics initiated by the transient H-bonding between Q513 and N414 and by extension

448 N482 which is predicted to slide out of the FMN binding pocket and recover back to its initial H-

449 bonding environment as Jα helix unfolds. Several different time constants have been reported for

450 the rate at which Jα helix unfolds. Transient grating (TG) spectroscopy, which is a diffusion

451 dependent signal, demonstrated that the helix unfolds in 2 steps in which the Jα helix undocks

452 from the β-sheet in 90 µs and has fully unfolded in 1-2 ms.[55,56] Here, we report a 313 µs time

453 constant for Jα helix unfolding which is complete by 1 ms based on comparison of the TRIR and

454 steady state FTIR difference spectra (**Figure 7**, **Supplementary Figure S5**) and is comparable to

455 previously reported value of 240 µs from Konold et al.[31] In contrast the Sig EAS of the N414A

456 mutant evolves more rapidly with a 93 µs time constant and is consistent with Q513 rotating back

457 to H-bond to FMN C4=O and N482 sliding back to H-bond to FMN C2=O faster than wild-type.

458 Therefore, we propose a novel role of N414 in which the side chain modulate the longer µs kinetics

459 of the LOV activation pathway.

460

461
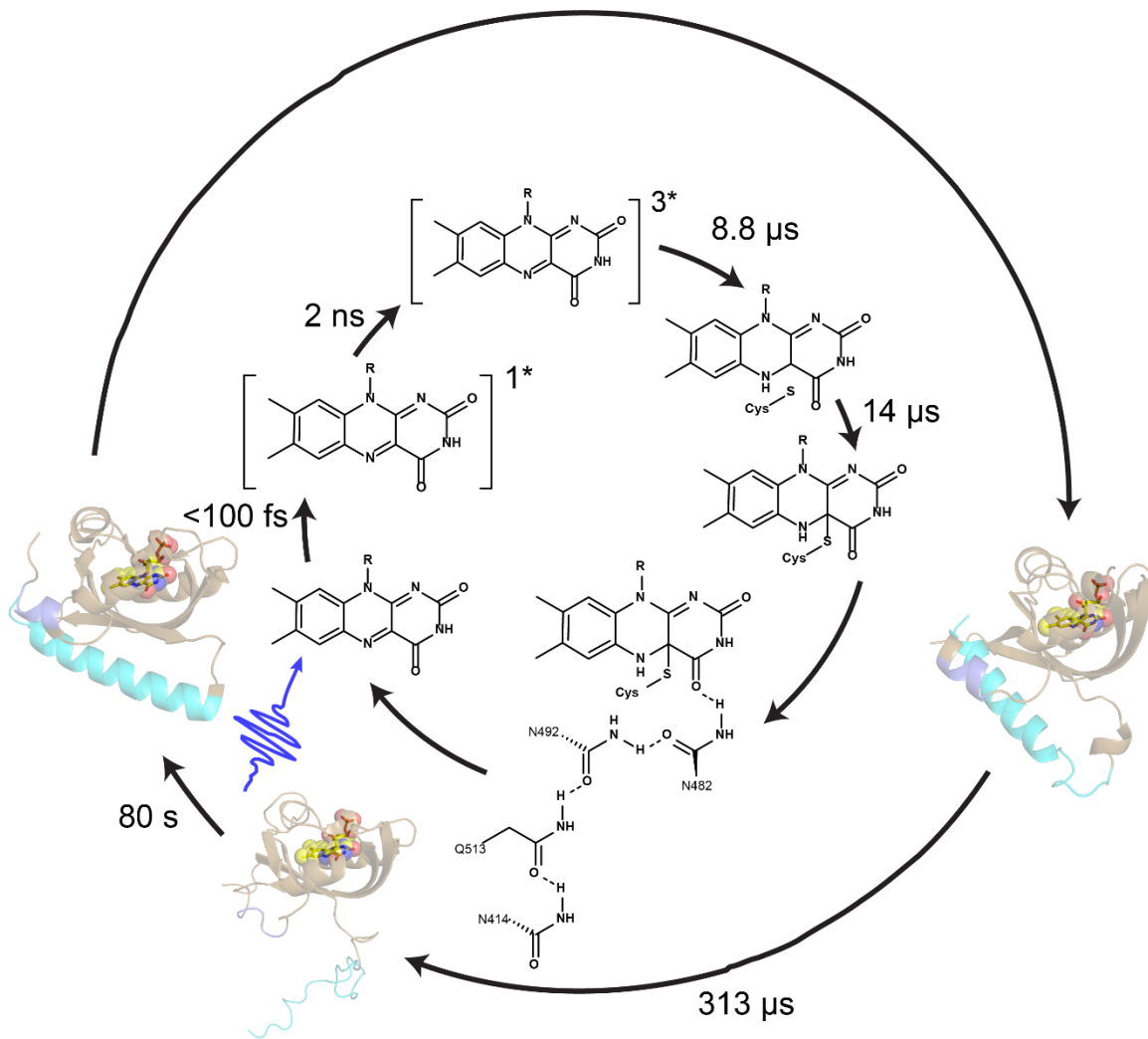
Figure 7: Phases of AsLOV2 activation with experimental time constants. Chromophore dynamics primarily occur on the ultrafast timescale while changes in the protein matrix occur much later with full Jα helix unfolding occurring with a time constant of 313 µs.

465

466

467 **Experimental**

468 *Molecular Dynamics Simulations*

469 Molecular dynamics (MD) simulations were used to analyze the structural dynamics of AsLOV2

470 starting from the X-ray structure of AsLOV2 in the light state. Solution NMR spectroscopy has

471 shown that the AsLOV2 Jα helix is unfolded in the light state. However, this helix is still folded

472 in the X-ray structure of the AsLov2 light state which is thought to be due to crystal contacts

473 between protein molecules. Thus, the dark state X-ray structure is an ideal starting point for

474 monitoring Jα helix unfolding since the folded helix should be the most stable species in solution.

475

476 *Parameter Development for the Flavin Cofactor:* Parameter generation proceeded in 2 parts. First,

477 a library file corresponding to the flavin alone was created. Coordinates were extracted from

478 protein data bank (PDB) 2V1B for AsLOV2 in the light state.[8] All atoms were deleted except for

479 those of the flavin. Chimera was used to add hydrogen atoms, and the hydrogen atom added to

480 atom C4A was then deleted since this is the site of Cys adduct formation.[34] These coordinates

481 were loaded into the Amber antechamber module using a charge of -3 to generate AM1BCC partial

482 charges and assign atom types for use with the GAFF2 general force field.[35] The resulting mol2

483 file was loaded into Amber parmchk2 to create a frcmod file, which was then loaded with the mol2

484 file into Amber tleap to create an Amber library file for the flavin. This provided the library files

485 appropriate for the structure of the flavin residue, ready to connect to the protein at C450.

486 However, the force field parameters do not correspond to the state following formation of the

487 adduct after light activation and additional steps were needed.

488 The next step involved generation of force field parameters for the flavin in the light-

489 activated adduct state. The process above was repeated except that the coordinates retained from

27

490   2V1B included the flavin as before, along with the SG and CB atoms from C450. Chimera was

491   used to add hydrogen atoms, resulting in a methyl capping group at the position of the C450 CB.

492   Antechamber was used to generate AM1BCC partial charges and GAFF2 atom types. Parmchk2

493   and tleap were used to create the Amber library file for the flavin attached to the SG and CB. Then,

494   the partial charges and atom types obtained in this step were copied to the atoms in the library file

495   obtained using only the flavin (described above), such that the final library file included only flavin

496   atoms, ready to accept a bond from C450, but with atom types and partial charges appropriate for

497   the state following adduct formation with C450. The bond angle and dihedral parameters used

498   were those obtained from GAFF2 using the flavin connected to the SG and CB atoms. Force field

499   parameters for the GAFF2↔ff14SB interface across C4A-SG were obtained by adopting the

500   parameters assigned by GAFF2 using the flavin+SG+CB fragment. This parameter file was edited

501   to change the atom types for the SG and CB atoms from those obtained using antechamber to those

502   appropriate for Cys in the ff14SB protein force field (c3 → 2C, ss → S). In this manner the protein

503   force field was applied inside Cys, but parameters for the Cys-flavin linkage (FMN-C) were

504   adopted from GAFF2. Finally, since the Cys backbone CA atom was not present in the larger

505   flavin fragment but is connected to the flavin through a dihedral term, parameters for the dihedral

506   C3-S-2C-CX (corresponding to atom names C4A-SG-CB-CA) were adapted from C3-S-C3-C3 in

507   GAFF2. The resulting library file and force field parameter file for the flavin in the light-activated

508   state are included as Supporting Information.

509

510   *Initial Modeling of FMN-C into the Dark State Structure:* Coordinates for AsLOV2 in the dark

511   state were obtained from PDB ID 2V1A.[8] Glycerol molecules were removed and 143 structured

512   water molecules were retained. Hydrogen atoms were added and the system was solvated in a

513   truncated octahedral box using a buffer of 8 Å minimum between any solute atom and the box

514   boundary, resulting in addition of 5014 water molecules. The OPC 4-point water model was

515   employed,[36] the parameters described above were used for the flavin, and the ff14SBonlysc protein

516   force field was used.[37] This model includes the side chain updates from ff14SB,[37] but not the

517   empirical backbone corrections included in that model for use with TIP3Pwater.[38] A covalent

518   bond was added between the SG atom of C450 and the C4A atom of the flavin, corresponding to

519   the bond that forms upon light activation.

520

521   *Equilibration of the FMN-C AsLOV2 Model:* Minimization and equilibration were carried out

522   using Amber version 16.[39,40] Initial minimization was performed for 100000 steps with restraints

523   on all atoms except hydrogens, water, C450 and the flavin. The restraint force constant was 100

524   $kcal \cdot mol^{-1} \cdot Å^{-2}$. Next, the system was heated from 100 K to 298 K over 1 ns in the NVT ensemble,

525   with a time step of 1 fs and SHAKE on all bonds including hydrogen. A nonbonded cutoff of 8 Å

526   was used, with long-range electrostatics included by the particle mesh Ewald method.[41] The same

527   restraints were maintained. Temperature was maintained using a Langevin thermostat with γ set

528   to 1.0. Next, pressure and density were relaxed using 1ns NPT simulation at 298 K with a strong

529   pressure coupling constant of 0.1 and all other parameters maintained from the prior step. Next, 1

530   ns MD was performed using the same protocol but with restraint force constant reduced to 10.0

531   and pressure coupling constant increased to 0.5. Next, minimization was performed for 10000

532   steps after removing all restraints except those on protein backbone CA, N and C atoms and no

533   restraints on C450. Next, 1 ns MD in the NPT ensemble at 298 K was performed using the same

534   protocol as above, with restraints only on backbone CA, N and C atoms excepting C450. The

535   restraint force constant was then reduced from 10.0 to 1.0 and an additional 1 ns MD was carried

29

536 out, followed by 1 ns MD with restraint force constant reduced to 0.1. Finally, 1 ns fully

537 unrestrained MD was performed with NPT at 298 K.

538

539 *Production runs:* Production runs followed the same protocols as equilibration, except that

540 hydrogen mass repartitioning was used to enable a 4 fs time step as has been described elsewhere.[42]

541 The simulation was performed on NVIDIA GPUs using the CUDA version of Amber.[43] MD was

542 continued until approximately 7.5 microseconds of dynamics were generated.

543

544 *Analysis:* Analysis of the MD simulation output was performing using the cpptraj module of

545 Amber,[44] along with custom python scripts.

546

547 *Site-directed Mutagenesis:* The N414A and N414Q mutations in AsLOV2 were created in the

548 pET15b-AsLOV2 and pHis-Gβ1-Parallel-AsLOV2 constructs using the QuickChange method and

549 KOD HotStart polymerase (Novagen).

550

551 *Expression and Purification of AsLOV2 for TRIR:* AsLOV2 and N414 mutants were expressed

552 and purified as described previously.[32] BL21(DE3) competent cells were transformed by heat

553 shock at 42°C with pET15b-AsLOV2 (wild-type or mutant) and the plated on LB-Agar plates

554 containing 200 µg/mL ampicillin. Following overnight incubation at 37°C, single bacterial

555 colonies were used to inoculate 10 mL of 2X-YT media containing 200 µg/mL ampicillin. After

556 overnight incubation at 37°C in an orbital shaker (250 RPM), the 10 mL cultures were used to

557 inoculate 1 L of 2X-YT media supplemented with 200 µg/mL ampicillin. The cultures were

558 incubated at 37°C in an orbital shaker (250 RPM) until the OD_{600} reached ~0.8-1.0 at 37°C and

559   protein expression was then induced by addition of 1 mM IPTG (Gold Biosciences). Protein

560   expression was allowed to proceed overnight at 18°C in an orbital shaker (250 RPM).

561   Cells from the 1 L cultures were harvested by centrifugation at 5,000 RPM (4°C) and

562   resuspended in 40 mL of 20 mM Tris buffer pH 8.0 containing 150 mM NaCl. The resuspended

563   cells were lysed by sonication and cell debris was removed by ultracentrifugation at 40,000 RPM

564   for 1 h (4°C). The clarified lysate was the loaded onto a 5 mL HisTrap FF column equilibrated

565   with resuspension buffer. The column was then washed with 100 ml of resuspension buffer

566   containing 20 mM imidazole, and protein was eluted with resuspension buffer containing 500 mM

567   imidazole. Fractions containing protein were pooled, concentrated to a volume of 5 mL using a 10

568   kDa MWCO concentrator (Amicon), and loaded onto a Superdex-75 column equilibrated with 20

569   mM Tris buffer pH 7.6, containing 150 mM NaCl. The protein was concentrated to 200 µM using

570   10 kDa MWCO concentrator and lyophilized for storage and prior to exchange into D_2O for the

571   TRIR measurements. Purity was >95% by SDS-PAGE.

572

573   *Expression and purification of 15N labelled AsLOV2:* Isotope labeling of AsLOV2 was performed

574   using the pHis-Gβ1-Parallel1 expression vector containing the DNA encoding wild-type AsLOV2

575   or the N414A or N414Q mutants (pHis-Gβ1-Parallel-AsLOV2). Protein expression and

576   purification were performed as described previously with some modifications.[9] Briefly,

577   BL21(DE3) cells were transformed by heat shock at 42°C with pHis-Gβ1-Parallel-AsLOV2 and

578   plated on LB-agar plates supplemented with 100 µg/mL ampicillin (Gold Biosciences). After

579   incubation overnight at 37°C, a single colony was used to inoculate 10 mL of 2X-YT media

580   containing 100 µg/mL ampicillin. After overnight incubation at 37°C in an orbital shaker

581   (250RPM), cells were harvested by centrifugation and rinsed by resuspension in 2x 10 mL volumes

582 of M9 salts followed by centrifugation. The rinsed cells were then used to inoculate 1 L of M9

583 medium supplemented with 1 g/L ^{15}N-NH$_4$Cl (Cambridge Isotope Labs), 4 g/L dextrose, 1X MEM

584 vitamins, 1 mM MgSO$_4$, 10% glycerol, and 100 µg/mL ampicillin. Bacterial cultures were

585 incubated at 37°C in an orbital shaker (250 RPM) until the culture reached an OD$_{600}$ of ~0.6-0.8.

586 Protein expression was induced by adding IPTG to a final concentration of 1 mM followed by

587 incubation at 18°C overnight (14-18 hours) in an orbital shaker (250 RPM).

588 Bacterial cells were harvested by centrifugation at 5,000 RPM for 10 min at 4°C, and the

589 cell pellet was subsequently resuspended in 20 mM Tris buffer pH 8.0 containing 150 mM NaCl

590 buffer. Cells were lysed by sonication and cell debris was removed by ultracentrifugation at

591 40,000 RPM for 1 h and 4°C. All subsequent purification steps were carried out on an AKTA

592 FPLC (Pharmacia Biosciences). The clarified lysate was loaded onto a 5 mL HisTrap FF Ni-NTA

593 column (GE) equilibrated with the resuspension buffer. The column was subsequently washed

594 with resuspension 100 mL buffer containing 20 mM imidazole, and protein was eluted using

595 resuspension buffer containing 500 mM imidazole. Fractions containing protein were pooled and

596 desalted to remove imidazole by gel filtration on a 50 mL BioScale P-6 column (BioRad) using

597 resuspension buffer as the eluant.

598 The Gβ1-His tag was removed using 1 mg of His-TEV protease per 30 mg of protein. Gβ1-

599 His tag AsLov2 was incubated with His-TEV protease overnight at 4°C on a rocking platform.

600 The Gβ1-His tag and His-TEV were separated from AsLOV2 using a 5 mL HisTrap FF column

601 equilibrated with 20 mM Tris buffer pH 8.0 containing 150 mM NaCl. Fractions containing

602 AsLOV2 were collected, pooled, and concentrated to 2 mL using a 10 kDa MWCO concentrator

603 (Amicon), and the protein was then exchanged into 50 mM sodium phosphate buffer pH 7.0

604 containing 150 mM NaCl and 6 mM sodium azide by size-exclusion chromatography on Superdex-

605   75 16/60 column equilibrated with the phosphate buffer. The protein was concentrated to 500 µM

606   using a 10 kDa MWCO concentrator for the NMR spectroscopy experiments. Protein purity was

607   >95% by SDS-PAGE.

608

609   *Time-Resolved Multiple Probe Spectroscopy (TRMPS):* TRIR spectroscopy was carried out at the

610   Central Laser Facility (Harwell, UK) using the Time resolved multiple probe spectroscopy

611   approach (TRMPS) which has been described previously.[45,46] Mid-IR probe light was generated

612   using an OPA with a DFG stage pumped by a Ti:Sapphire laser and the signal and idler outputs

613   were mixed to generate the broadband probe centered at ~1550 cm^{-1} with a pulse duration of <100

614   fs at a repetition rate of 10 kHz. The 450 nm visible pump with 100 µm spot size and 800 nJ

615   energy was generated by a second Ti:Sapphire laser pumped OPA (SpectraPhysics Ascend and

616   Spitfire) with a pulse duration of ~100 fs and a 1 kHz repetition rate. Probe light was detected

617   using two 128-pixel MCT detectors to give ~400 cm^{-1} spectral bandwidth. The spectra were

618   calibrated to polystyrene film giving a resolution of 3 cm^{-1}. The approach used in this work was

619   modified to include a chopper to modulate the repetition rate of the pump laser from 1 kHz to 500

620   Hz such that a pump-off subtraction of the baseline was performed on each spectrum prior to

621   excitation, eliminating fixed pattern noise and enabling longer time delay acquisitions.[47] Protein

622   samples were concentrated to 1 mM using a 10 kDa MWCO concentrator and ~1 mL of this

623   solution was loaded into a Harrick cell modified for low volume flow at a rate of 1 mL/min. A 50

624   µm spacer was used between two CaF_2 windows and the sample cell was rastered to ensure fresh

625   sample for each laser shot. Time resolved data were globally analyzed and fit to a sequential

626   exponential decay model using the Glotaran Software Package.[48]

627

628 *^1H-^{15}N HSQC NMR:* Multidimensional ^1H-^{15}N HSQC NMR spectroscopy was performed on a

629 Bruker Avance III HD 800 MHz Spectrometer. Both dark and light state spectra of wild-type and

630 mutant AsLOV2 proteins were acquired as previously described.[9] The light state of AsLOV2 was

631 generated by illumination using a Coherent Sapphire Laser (488 nm, ~200 mW) focused into a

632 fiber optic wand that was submerged into the protein solution in the NMR tube. The power at the

633 end of the fiber was set to 50 mW and a shutter controlled by Bruker Topspin Software enabled

634 pulses of 120 ms prior to each transient.[49] Processing and analysis was performed using Bruker

635 TopSpin Software.

636

637 *LOVTRAP Cellular Assay:* InFusion cloning (Clontech) was used to attach iRFP to the N-terminus

638 of AsLOV2 (wild-type, N414A or N414Q mutants). The pHR lentivirus vector, ZDK insert and

639 AsLOV2 insert sequences were amplified using HiFi or GXL polymerase, subjected to infusion

640 cloning, and amplified using Stellar competent cells. Sequences were verified using restriction

641 digests and Sanger sequencing (GeneWiz).

642 Lenti-X 293T cells were used to generate virus for transfection and expression of

643 constructs. Cells were maintained in a 6-well plate containing 2 mL of DMEM supplemented with

644 10% FBS, 100 µg/mL penicillin/streptomycin, and 2 mM L-glutamine per well or T25 flasks

645 containing 5 mL of the same medium at 37° with 5% CO_2.

646 Lentiviral particles containing the iRFP-AsLOV2 construct or the ZDK p2a Fusion Red

647 construct were generated by transfecting Lenti-X 293T cells with the pHR-iRFP-AsLOV2 vector

648 or the pHR-ZDK-p2a-FusionRed together with the pCMV-dR8.91 and pMD2.G lenti-helper

649 plasmids in a 1.5:1.3:0.17 ratio, respectively. The helper plasmids were gifts from the Torono lab

650 via Addgene, and transfections were performed using Fugene transfection reagent (Promega). The

651   transfected Lenti-X 293T cells were incubated at 37° with 5% CO_2 for two days, after which the

652   media containing lentivirus particles was filtered through a 0.45 µm filter. Forty µL of 1 M HEPES

653   buffer pH 7.4 was then added to ~2 mL of the filtered media which was then stored at 4°C for two

654   weeks for immediate use or at -80°C for long term storage.

655   Prior to infection, LentiX 293Ts were plated at 50% confluency and incubated overnight to attach.

656   Five hundred µL of the viral media was then added to the cells. After incubation for 24 h at 37°C

657   with 5% CO_2, the cells were washed with fresh media and then incubated at 37°C with 5% CO_2

658   for another 24 h. Cells to be imaged were plated 12 h prior to imaging in 96-well, black-walled,

659   glass bottomed plates (InVitro Scientific) coated with 100 µl of 10 µg/mL fibronectin diluted in

660   PBS which was rinsed off with PBS prior to plating cells in full media. Confocal microscopy was

661   performed on a Nikon Eclipse Ti Microscope equipped with a linear motorized stage (Pior), CSU-

662   X1 spinning disk (Yokogawa), using 561 nm (ZDK-p2a-FusionRed) and 650 nm (iRFP-AsLOV2)

663   modules (Agilent) laser lines. Images were acquired using a 60x oil-immersion objective and an

664   iXon DU897 EMCCD camera. For FMN excitation, 447 nm light was provided by a LED light

665   source (Xcite XLED1) through a digital micromirror device (Polygon400, Mightex Systems) to

666   temporally control light inputs.

667   **Conclusion**

668   In conclusion, we have used multiple approaches to shed new light on key events in the

669   AsLOV2 photocycle immediately following Cys-FMN adduct formation, which occurs on the µs

670   timescale and is associated with changes in the protein matrix at sites that are distant from the

671   primary photochemistry. MD simulations reveal the formation of a transient hydrogen bond

672   between Q513 and N414, two conserved residues in the LOV2 domain family, upon rotation of

673   Q513. TRIR and NMR studies show that the structural dynamics are significantly decoupled from

674 FMN excitation in the N414A AsLOV2 mutant where the Jα helix is partially unfolded in the dark

675 state, leading to residual dark state activity. The structural studies have been complemented with

676 a cell-based assay which substantiate the critical role that N414 plays in transmitting information

677 from the chromophore to the Jα helix. Together these results represent a high-resolution picture of

678 the inner workings of a photosensory protein in which a glutamine lever induces microsecond

679 structural dynamics via H-bond pathways that link the FMN chromophore to the Jα helix.

680

References

696

697 (1) Shcherbakova, D. M.; Shemetov, A. A.; Kaberniuk, A. A.; Verkhusha, V. V. Natural

698 Photoreceptors as a Source of Fluorescent Proteins, Biosensors, and Optogenetic Tools.

699 *Annu. Rev. Biochem.* **2015**, *84* (1), 519–550.

700 (2) Christie, J. M.; Gawthorne, J.; Young, G.; Fraser, N. J.; Roe, A. J. LOV to BLUF:

701 Flavoprotein Contributions to the Optogenetic Toolkit. *Mol. Plant* **2012**, *5* (3), 533–544.

702 (3) Swartz, T. E.; Corchnoy, S. B.; Christie, J. M.; Lewis, J. W.; Szundi, I.; Briggs, W. R.;

703 Bogomolni, R. A. The Photocycle of a Flavin-Binding Domain of the Blue Light

704 Photoreceptor Phototropin. *J. Biol. Chem.* **2001**, *276* (39), 36493–36500.

705 (4) Kennis, J. T. M.; Crosson, S.; Gauden, M.; van Stokkum, I. H. M.; Moffat, K.; van

706 Grondelle, R. Primary Reactions of the LOV2 Domain of Phototropin, a Plant Blue-Light

707 Photoreceptor. *Biochemistry* **2003**, *42* (12), 3385–3392.

708 (5) Yee, E. F.; Diensthuber, R. P.; Vaidya, A. T.; Borbat, P. P.; Engelhard, C.; Freed, J. H.;

709 Bittl, R.; Möglich, A.; Crane, B. R. Signal Transduction in Light-Oxygen-Voltage

710 Receptors Lacking the Adduct-Forming Cysteine Residue. *Nat. Commun.* **2015**, *6*, 10079.

711 (6) Herrou, J.; Crosson, S. Function, Structure and Mechanism of Bacterial Photosensory

712 LOV Proteins. *Nat. Rev. Microbiol.* **2011**, *9* (10), 713–723.

713 (7) The PyMOL Molecular Graphics System, Version 2.0 Schrodinger, LLC.

714 (8) Halavaty, A. S.; Moffat, K. N- and C-Terminal Flanking Regions Modulate Light-Induced

715 Signal Transduction in the LOV2 Domain of the Blue Light Sensor Phototropin 1 from

716 Avena Sativa. *Biochemistry* **2007**, *46* (49), 14001–14009.

717 (9) Harper, S. M.; Neil, L. C.; Gardner, K. H. Structural Basis of a Phototropin Light Switch.

718 *Science* **2003**, *301* (5639), 1541–1544.

719   (10)   Nash, A. I.; Ko, W.; Harper, S. M.; Gardner, K. H. A Conserved Glutamine Plays a

720   Central Role in LOV Domain Signal Transmission and Its Duration. *Biochemistry* **2008**,

721   *47* (52), 13842–13849.

722   (11)   Nozaki, D.; Iwata, T.; Ishikawa, T.; Todo, T.; Tokutomi, S.; Kandori, H. Role of Gln1029

723   in the Photoactivation Processes of the LOV2 Domain in Adiantum Phytochrome3.

724   *Biochemistry* **2004**, *43* (26), 8373–8379.

725   (12)   Zayner, J. P.; Antoniou, C.; Sosnick, T. R. The Amino-Terminal Helix Modulates Light-

726   Activated Conformational Changes in AsLOV2. *J. Mol. Biol.* **2012**, *419* (1–2), 61–74.

727   (13)   Freddolino, P. L.; Gardner, K. H.; Schulten, K. Signaling Mechanisms of LOV Domains:

728   New Insights from Molecular Dynamics Studies. *Photochem. Photobiol. Sci.* **2013**, *12*,

729   1158–1170.

730   (14)   Lee, J.; Natarajan, M.; Nashine, V. C.; Socolich, M.; Vo, T.; Russ, W. P.; Benkovic, S. J.;

731   Ranganathan, R. Surface Sites for Engineering Allosteric Control in Proteins. *Science.*

732   **2008**, *322* (5900), 438–442.

733   (15)   Strickland, D.; Moffat, K.; Sosnick, T. R. Light-Activated DNA Binding in a Designed

734   Allosteric Protein. *Proc. Natl. Acad. Sci.* **2008**, *105* (31), 10709–10714.

735   (16)   Möglich, A.; Ayers, R. A.; Moffat, K. Design and Signaling Mechanism of Light-

736   Regulated Histidine Kinases. *J. Mol. Biol.* **2009**, *385* (5), 1433–1444.

737   (17)   Wu, Y. I.; Frey, D.; Lungu, O. I.; Jaehrig, A.; Schlichting, I.; Kuhlman, B.; Hahn, K. M. A

738   Genetically Encoded Photoactivatable Rac Controls the Motility of Living Cells. *Nature*

739   **2009**, *461* (7260), 104–108.

740   (18)   Winkler, A.; Barends, T. R. M.; Udvarhelyi, A. A.; Lenherr-Frey, D.; Lomb, L.; Menzel,

741   A.; Schlichting, I. Structural Details of Light Activation of the LOV2-Based Photoswitch

742   PA-Rac1. *ACS Chem. Biol.* **2015**, *10* (2), 502–509.

743   (19)   Guntas, G.; Hallett, R. a.; Zimmerman, S. P.; Williams, T.; Yumerefendi, H.; Bear, J. E.;

744   Kuhlman, B. Engineering an Improved Light-Induced Dimer (ILID) for Controlling the

745   Localization and Activity of Signaling Proteins. *Proc. Natl. Acad. Sci.* **2015**, *112* (1), 112–

746   117.

747   (20)   Niopek, D.; Wehler, P.; Roensch, J.; Eils, R.; Di Ventura, B. Optogenetic Control of

748   Nuclear Protein Export. *Nat. Commun.* **2016**, *7*, 1–9.

749   (21)   Strickland, D.; Lin, Y.; Wagner, E.; Hope, C. M.; Zayner, J.; Antoniou, C.; Sosnick, T. R.;

750   Weiss, E. L.; Glotzer, M. TULIPs: Tunable, Light-Controlled Interacting Protein Tags for

751   Cell Biology. *Nat. Methods* **2012**, *9* (4), 379–384.

752   (22)   Johnson, H. E.; Toettcher, J. E. Illuminating Developmental Biology with Cellular

753   Optogenetics. *Curr. Opin. Biotechnol.* **2018**, *52*, 42–48.

754   (23)   Nakagawa, S.; Weingart, O.; Marian, C. M. Dual Photochemical Reaction Pathway in

755   Flavin-Based Photoreceptor LOV Domain: A Combined Quantum-Mechanics/Molecular-

756   Mechanics Investigation. *J. Phys. Chem. B* **2017**, *121* (41), 9583–9596.

757   (24)   Chang, X.-P.; Gao, Y.-J.; Fang, W.-H.; Cui, G.; Thiel, W. QM/MM Study on the

758   Photoreactions of Dark- and Light-Adapted States of a Blue-Light YtvA LOV

759   Photoreceptor. *Angew. Chemie Int. Ed.* **2017**.

760   (25)   Peter, E.; Dick, B.; Baeurle, S. A. Mechanism of Signal Transduction of the LOV2-Jα

761   Photosensor from Avena Sativa. *Nat. Commun.* **2010**, *1* (8), 122.

762   (26)   Kopka, B.; Magerl, K.; Savitsky, A.; Davari, M. D.; Röllen, K.; Bocola, M.; Dick, B.;

763   Schwaneberg, U.; Jaeger, K. E.; Krauss, U. Electron Transfer Pathways in a Light,

764   Oxygen, Voltage (LOV) Protein Devoid of the Photoactive Cysteine. *Sci. Rep.* **2017**, *7*

765   (1), 1–16.

766   (27)   Zayner, J. P.; Sosnick, T. R. Factors That Control the Chemistry of the LOV Domain

767   Photocycle. *PLoS One* **2014**, *9* (1), e87074.

768   (28)   Alexandre, M. T. A.; van Grondelle, R.; Hellingwerf, K. J.; Kennis, J. T. M.

769   Conformational Heterogeneity and Propagation of Structural Changes in the LOV2/Jα

770   Domain from Avena Sativa Phototropin 1 as Recorded by Temperature-Dependent FTIR

771   Spectroscopy. *Biophys. J.* **2009**, *97* (1), 238–247.

772   (29)   Yamamoto, A.; Iwata, T.; Sato, Y.; Matsuoka, D.; Tokutomi, S.; Kandori, H. Light Signal

773   Transduction Pathway from Flavin Chromophore to the Jα Helix of Arabidopsis

774   Phototropin1. *Biophys. J.* **2009**, *96* (7), 2771–2778.

775   (30)   Zayner, J. P.; Mathes, T.; Sosnick, T. R.; Kennis, J. T. M. Helical Contributions Mediate

776   Light-Activated Conformational Change in the LOV2 Domain of Avena Sativa

777   Phototropin 1. *ACS Omega* **2019**, *4* (1), 1238–1243.

778   (31)   Konold, P. E.; Mathes, T.; Weiβenborn, J.; Groot, M. L.; Hegemann, P.; Kennis, J. T. M.

779   Unfolding of the C-Terminal Jα Helix in the LOV2 Photoreceptor Domain Observed by

780   Time-Resolved Vibrational Spectroscopy. *J. Phys. Chem. Lett.* **2016**, *7* (17), 3472–3476.

781   (32)   Gil, A. A.; Laptenok, S. P.; French, J. B.; Iuliano, J. N.; Lukacs, A.; Hall, C. R.;

782   Sazanovich, I. V.; Greetham, G. M.; Bacher, A.; Illarionov, B.; Fischer, M.; Tonge, P. J.;

783   Meech, S. R. Femtosecond to Millisecond Dynamics of Light Induced Allostery in the

784   Avena Sativa LOV Domain. *J. Phys. Chem. B* **2017**, *121* (5), 1010–1019.

785   (33)   Iuliano, J. N.; Gil, A. A.; Laptenok, S. P.; Hall, C. R.; Tolentino Collado, J.; Lukacs, A.;

786   Hag Ahmed, S. A.; Abyad, J.; Daryaee, T.; Greetham, G. M.; Sazanovich, I. V.;

787   Illarionov, B.; Bacher, A.; Fischer, M.; Towrie, M.; French, J. B.; Meech, S. R.; Tonge, P.

788   J. Variation in LOV Photoreceptor Activation Dynamics Probed by Time-Resolved

789   Infrared Spectroscopy. *Biochemistry* **2018**, *57* (5), 620–630.

790   (34) Pettersen, E. F.; Goddard, T. D.; Huang, C. C.; Couch, G. S.; Greenblatt, D. M.; Meng, E.

791   C.; Ferrin, T. E. UCSF Chimera- A Visualization System for Exploratory Research and

792   Analysis. *J. Comput. Chem.* **2004**, *25* (13), 1605–1612.

793   (35) Wang, J.; Wolf, R. M.; Caldwell, J. W.; Kollman, P. A.; Case, D. A. Development and

794   Testing of a General Amber Force Field. *J. Comput. Chem.* **2004**, *25* (9), 1157–1174.

795   (36) Izadi, S.; Anandakrishnan, R.; Onufriev, A. V. Building Water Models: A Different

796   Approach. *J. Phys. Chem. Lett.* **2014**, *5* (21), 3863–3871.

797   (37) Maier, J. A.; Martinez, C.; Kasavajhala, K.; Wickstrom, L.; Hauser, K. E.; Simmerling, C.

798   Ff14SB: Improving the Accuracy of Protein Side Chain and Backbone Parameters from

799   Ff99SB. *J. Chem. Theory Comput.* **2015**, *11* (8), 3696–3713.

800   (38) Jorgensen, W. L.; Chandrasekhar, J.; Madura, J. D.; Impey, R. W.; Klein, M. L.

801   Comparison of Simple Potential Functions for Simulating Liquid Water. *J. Chem. Phys.*

802   **1983**, *79* (2), 926–935.

803   (39) Case, D. A.; Cheatham, T. E.; Darden, T.; Gohlke, H.; Luo, R.; Merz, K. M.; Onufriev,

804   A.; Simmerling, C.; Wang, B.; Woods, R. J. The Amber Biomolecular Simulation

805   Programs. *J. Comput. Chem.* **2005**, *26* (16), 1668–1688.

806   (40) D.A. Case, R.M. Betz, D.S. Cerutti, T.E. Cheatham, III, T.A. Darden, R.E. Duke, T.J.

807   Giese, H. G.; A.W. Goetz, N. Homeyer, S. Izadi, P. Janowski, J. Kaus, A. Kovalenko, T.S.

808   Lee, S. LeGrand, P. Li, C.; Lin, T. Luchko, R. Luo, B. Madej, D. Mermelstein, K.M.

809   Merz, G. Monard, H. Nguyen, H.T. Nguyen, I.; Omelyan, A. Onufriev, D.R. Roe, A.

810   Roitberg, C. Sagui, C.L. Simmerling, W.M. Botello-Smith, J. S.; R.C. Walker, J. Wang,

811   R.M. Wolf, X. Wu, L. X. AMBER 2016. University of California, San Francisco.

812 (41) Darden, T.; York, D.; Pedersen, L. Particle Mesh Ewald: An N ·log(N) Method for

813   Ewald Sums in Large Systems. *J. Chem. Phys.* **1993**, *98* (12), 10089–10092.

814 (42) Hopkins, C. W.; Le Grand, S.; Walker, R. C.; Roitberg, A. E. Long-Time-Step Molecular

815   Dynamics through Hydrogen Mass Repartitioning. *J. Chem. Theory Comput.* **2015**, *11* (4),

816   1864–1874.

817 (43) Salomon-Ferrer, R.; Götz, A. W.; Poole, D.; Le Grand, S.; Walker, R. C. Routine

818   Microsecond Molecular Dynamics Simulations with AMBER on GPUs. 2. Explicit

819   Solvent Particle Mesh Ewald. *J. Chem. Theory Comput.* **2013**, *9* (9), 3878–3888.

820 (44) Roe, D. R.; Cheatham, T. E. PTRAJ and CPPTRAJ: Software for Processing and Analysis

821   of Molecular Dynamics Trajectory Data. *J. Chem. Theory Comput.* **2013**, *9* (7), 3084–

822   3095.

823 (45) Greetham, G. M.; Burgos, P.; Qian, C.; Clark, I. P.; Codd, P. S.; Farrow, R. C.; George,

824   M. W.; Kogimtzis, M.; Matousek, P.; Parker, A. W.; Pollard, M. R.; Robinson, D. A.; Zhi-

825   Jun, X.; Towrie, M. ULTRA: A Unique Instrument for Time-Resolved Spectroscopy.

826   *Appl. Spectrosc.* **2010**, *64* (12), 1311–1319.

827 (46) Greetham, G. M.; Sole, D.; Clark, I. P.; Parker, A. W.; Pollard, M. R.; Towrie, M. Time-

828   Resolved Multiple Probe Spectroscopy. *Rev. Sci. Instrum.* **2012**, *83* (10), 103107.

829 (47) Fritzsch, R.; Greetham, G. M.; Clark, I. P.; Minnes, L.; Towrie, M.; Parker, A. W.; Hunt,

830   N. T. Monitoring Base-Specific Dynamics during Melting of DNA–Ligand Complexes

831   Using Temperature-Jump Time-Resolved Infrared Spectroscopy. *J. Phys. Chem. B* **2019**,

832   *123* (29), 6188–6199.

833 (48) Snellenburg, J. J.; Laptenok, S. P.; Seger, R.; Mullen, K. M.; Stokkum, I. H. M. van.

834   Glotaran: A Java -Based Graphical User Interface for the R Package TIMP. *J. Stat. Softw.*

835   **2012**, *49* (3).

836 (49) Nash, A. I.; McNulty, R.; Shillito, M. E.; Swartz, T. E.; Bogomolni, R. a; Luecke, H.;

837   Gardner, K. H. Structural Basis of Photosensitivity in a Bacterial Light-Oxygen-

838   Voltage/Helix-Turn-Helix (LOV-HTH) DNA-Binding Protein. *Proc. Natl. Acad. Sci. U.*

839   *S. A.* **2011**, *108* (22), 9449–9454.

840 (50) Harper, S. M.; Christie, J. M.; Gardner, K. H. Disruption of the LOV−Jα Helix Interaction

841   Activates Phototropin Kinase Activity. *Biochemistry* **2004**, *43* (51), 16184–16192.

842 (51) Wang, H.; Vilela, M.; Winkler, A.; Tarnawski, M.; Schlichting, I.; Yumerefendi, H.;

843   Kuhlman, B.; Liu, R.; Danuser, G.; Hahn, K. M. LOVTRAP: An Optogenetic System for

844   Photoinduced Protein Dissociation. *Nat. Methods* **2016**, *13* (9), 755–758.

845 (52) Losi, A.; Gardner, K. H.; Möglich, A. Blue-Light Receptors for Optogenetics. *Chem. Rev.*

846   **2018**, *118* (21), 10659–10709.

847 (53) Ganguly, A.; Thiel, W.; Crane, B. R. Glutamine Amide Flip Elicits Long Distance

848   Allosteric Responses in the LOV Protein Vivid. *J. Am. Chem. Soc.* **2017**, *139* (8), 2972–

849   2980.

850 (54) Kalvaitis, M. E.; Johnson, L. A.; Mart, R. J.; Rizkallah, P.; Allemann, R. K. A

851   Noncanonical Chromophore Reveals Structural Rearrangements of the Light-Oxygen-

852   Voltage Domain upon Photoactivation. *Biochemistry* **2019**, *58* (22), 2608–2616.

853 (55) Eitoku, T.; Nakasone, Y.; Matsuoka, D.; Tokutomi, S.; Terazima, M. Conformational

854   Dynamics of Phototropin 2 LOV2 Domain with the Linker upon Photoexcitation. *J. Am.*

855   *Chem. Soc.* **2005**, *127* (38), 13238–13244.

856 (56) Nakasone, Y.; Eitoku, T.; Matsuoka, D.; Tokutomi, S.; Terazima, M. Dynamics of
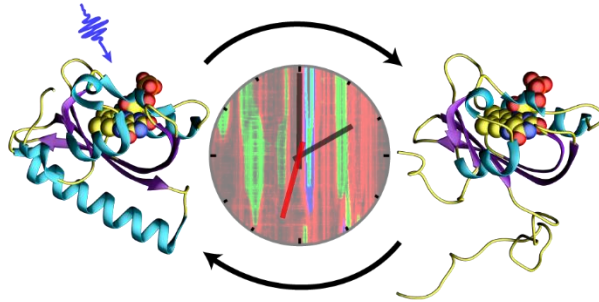
857   Conformational Changes of Arabidopsis Phototropin 1 LOV2 with the Linker Domain. *J.*

858   *Mol. Biol.* **2007**, *367* (2), 432–442.

859

Table of contents figure:

861

862

863